MODELING AMPLITUDE-MODULATION ATOMIC FORCE MICROSCOPY USING DIRECT-QUADRATURE TRANSFORMATION

BY

YUCHEN XU

THESIS

Submitted in partial fulfillment of the requirements
for the degree of Master of Science in Mechanical Engineering
in the Graduate College of the
University of Illinois at Urbana-Champaign, 2020

Urbana, Illinois

Adviser:

Professor Srinivasa M Salapaka

ABSTRACT

This thesis presents modeling of amplitude-modulated atomic force microscopy. The existing models of AM-AFM rely on averaging of dynamic models, where second order ordinary differential equations are considered with sinusoidal forcing which are perturbed with small forces that model cantilever tip and sample interactions. The resulting models that relate cantilever amplitude to sample motions are complex and inaccurate. These challenges have forced using model-free control design approaches, which can provide only limited performance; especially limited in disturbance rejection bandwidth, which severely impede imaging quality and bandwidth. The approach proposed in this thesis relies on deriving models in a rotating frame, whereby the resulting models are simple and accurate. Here, the proposed model is derived using direct-quadrature (dq) frame (rotating frame) transformation, which is commonly used in electrical power systems literature to describe dynamical systems driven by near-harmonic oscillating signals. This coordination transformation requires at least two-dimensional coordinate system; accordingly a fictitious AFM system is assumed running in parallel with the original AFM system. In the rotating frame, the trajectories are represented by dynamics of phasors, where the orthogonal components of these phasors closely relate to the amplitudes of the solutions of the real and fictitious systems. The resulting dynamical model is simple which can be used to enable model-based analysis and control design. We demonstrate that this model provides an accurate (5.5 % estimation error) over a bandwidth of up to 2.5% of the cantilever resonance frequency. This is sufficient for control design since current AM-AFM implementations typically use bandwidths in the range of 0.01%-0.1% of the cantilever resonance frequency. We modify our design with extra signal processing of our amplitude estimate, where we designed a notch filter to gives a to reduce the unwanted higher harmonics and other frequency components that hinder the estimation accuracy. The notch filter design reduced the unwanted high frequency components by over 80% giving much more accuracy with amplitude and phase estimation errors less than 1.5% over a bandwidth of 2.5 % of cantilever resonance frequency. The resulting model is also in a structure more suitable for sample physical property estimation than existing models such as Krylov-Bogoliubov-Mitropolsky models.

To my parents

ACKNOWLEDGMENTS

First, I would like to thank my advisor, Professor Srinivasa M. Salapaka for his patient support, careful teaching and responsible guidance throughout my master study at UIUC. The discussions with Professor Salapaka are always very constructive and inspired me a lot.

I would also like to thank my research colleague Ram Sai Gorugantu. As the colleague who is also working on AFM, Ram introduced me all devices used in the lab, like Labview and FPGA. Ram also helped me a lot with H_∞ controller design. Although not everything Ram helped me are included in this thesis, those are still helpful skills for my life and helpful for a thorough understanding of AFM.

I also want to express my appreciate to MRL staff who are in charge of AFM, Kathy Walsh and Jessica Spear. They gave me initial trainings on AFM operation at the starting stage of my research. They are very patient and helpful for anyone who want to use the device.

I want to express my most special appreciation to my parents. They always cares me and support me at the most content during my life. Although disagreement always appears between us, they are always trying to offer me the best solution they can think of. They not only supported me during my two years of master study, it was because of their support throughout my life that I can now do graduate study here in a top university.

TABLE OF CONTENTS

LIST OF FIGURES

LIST OF ABBREVIATIONS

AFM	Atomic Force Microscopy
AM-AFM	Amplitude Modulation Atomic Force Microscopy
DMT	Derjaguin-Müller-Toporov
FM-AFM	Frequencyt Modulation Atomic Force Microscopy
InvOLS	Optical Lever Detection Sensitivity
KBM	Krylov-Bogoliubov-Mitropolskii
PID	Proportional Integral Derivative
SNR	Signal-to-Noise Ratio
STM	Scanning Tunneling Microscope

CHAPTER 1

INTRODUCTION

This thesis presents a new model that describes the dynamics of the amplitude-modulated atomic force microscopy (AM-AFM), also known as the tapping mode atomic force microscopy. In tapping-mode AFM, a microcantilever is made to oscillate at a frequency near its resonance frequency and brought near a sample to be imaged. The oscillation amplitude changes as a result of interaction forces between the atoms on the cantilever tip and the atoms on the samples features that are closest to the tip. Since the interaction forces depend sharply on the vertical distance between the cantilever tip and the sample, the resulting amplitude changes carry the information of the sample. This information is collected at different positions as the sample is moved laterally under the cantilever.

Tip-sample interaction forces are extremely sensitive to the distances between them; and reliable measurements are not obtained even if the tip-sample separation is beyond a couple of nanometers. Since it is extremely difficult to maintain the lateral motion of the sample, which can be in hundreds of microns, within this separation range from the cantilever-tip, it is practically infeasible to obtain sample-profiles directly from amplitude measurements. In order to overcome this obstacle, in tapping mode, a control system is used to maintain a constant separation between the tip and the sample. This is done by moving the sample or cantilever beam up and down in a controlled manner such that these motions compensate for the effects of sample features on the oscillation amplitudes. In this mode of operation, the cantilever tip is maintained in the desirable range. Here the control effort that moves the sample up and down to cancel the effects of sample features can be used as a measure of the sample profile [1].

A main impediment to the control design is that the dynamic model that represents the relationship between the motion of the sample features and the cantilever-tip oscillation amplitude is nonlinear and difficult to model. This complexity also implies that the *plant model* - the model between the control input for sample motion and the output - the oscillation amplitude of the cantilever tip is difficult to obtain. There are phenomenological models that are available but these models are complex and do not accurately reflect true experimental

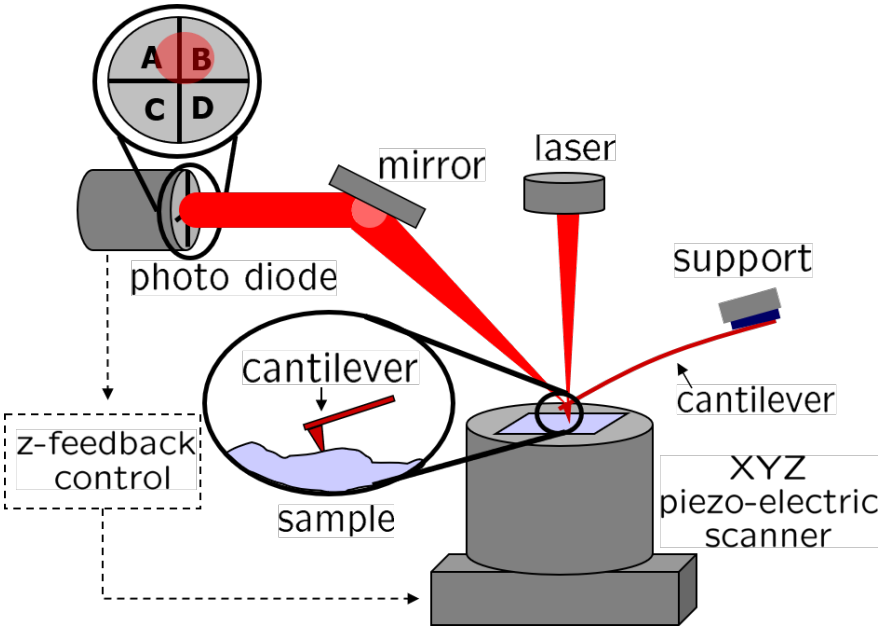

Figure 1.1: A diagram of atomic force microscope [11]

conditions. Many of these models, such as Derjaguin-Muller-Toporov (DMT) model [2] that models tip-sample interaction, make assumptions on the tip and sample properties, which are not easy to enforce or ascertain on real experiments. Even under assumptions of such tip-sample interaction force models, the dynamical models that relate oscillation amplitude and the motion of the sample features are complex. Some research runs numerical simulations based on DMT models. Although important relations between tip-sample distance and frequency responses under different conditions can be found, no straightforward mathematical relations are found[3]. Other methods, such as the Krylov-Bogoliubov-Mitropolskii (KBM) method[4], which is based on averaging theory and perturbation methods that assumes tip-sample interaction models as DMT, results in describing dynamic models for amplitude and phase dynamics. However these models are limited - they provide some qualitative insights but do not model appropriately experimental conditions, or are very complex to design control systems for [4]. The state-of-the art is that model-free control designs, typically proportional integral derivative (PID) control designs, are used to regulate the cantilever oscillation amplitude since the existing models are very complex and do not accurately model the experimental system. Applying model-free control designs also bring another difficulties: estimating the physical properties of the materials are more difficult. Various efforts are done to extract information from phase and amplitude data [6][7][8]. However, those methods are usually limited to soft materials that can give large enough displacements, like soft polymals and biological tissues, and they requires complex calculations and information more than 1st harmonic components of the cantilever oscillation are required. Another important impedi-

ment to model-based control design is that the resonance frequencies of the microcantilever systems are very high - on the order of the 100 kHz, which makes sophisticated fast electronic systems inevitable for implementing control designs based on them.

In this thesis, we bridge this gap. We provide a new model that describes amplitude-sample control dynamics, which is relatively simple and amenable for control design. We demonstrate through simulations, how our model reconstructs the amplitude signal. Our method leverages on an analogy with electrical circuits and on models that describe them. Many electrical grids require regulation amplitude of an ac bus - analogous to regulating the oscillation amplitude of the cantilever. In power systems, *phasors* are used to represent dynamics of *near* harmonic signals, where phasors can be thought as vectors in rotating-coordinate frames[9]. Here the projections of the magnitude on a specified axis typically represent the required amplitude signals. This analogy and framework is described in Chapter 3.

In power systems these methods introduce direct-quadrature (dq) coordinates where projections of the phasors on the d-axis represents real or *active* components and projections on the q-axis represents the *reactive* components. The reactive components (for instance reactive power) are typically fictitious quantities (such as reactive power) though they have physical interpretations. However these models in dq framework greatly simplify the analysis when compared to analysis only on the real (d) axis. To enable this analogy, we introduce fictitious cantilever dynamics equations. We demonstrate how considering the systems of the real and fictitious systems together makes the resulting analysis simpler than considering the real system by itself.

More precisely, we consider rotating coordinate frame (rotating with the oscillation frequency), where the horizontal d-axis represents the oscillation amplitude of the real cantilever system and the orthogonal q-axis represents the amplitude of the fictitious system. In this extended model framework, we show that the resulting cantilever amplitude dynamics are accurate over a large bandwidth. The amplitude and phase signals retrieved from this model can fit the actual amplitude nicely with heights varying at up to 2 kHz. One drawback of this model is that excessive high frequency component will appear during some transient process. A filter can be combined with the model to reduce the unwanted high frequency components to less than 16% of the original amount

On the control perspective, the resulting model is also in a structure that is convenient to introduce a control effort by dither piezo, and take the nonlinear atomic interaction forces as external disturbance, then do a model based control design similar to the work done by[10].

The control input lies in a nonlinear function if a control through cantilever beam head or sample stage is desired just similar to the control structure proposed by [10].

This thesis is organized as follows. Chapter 2 gives a thorough introduction of AFM as a device. On the Chapter 3, the dq-frame transformation is introduced, and simulation results of estimating amplitude and phases through dq-frame transformation are shown. Comparison with KBM method is also given in the Chapter 3.

CHAPTER 2

AFM SYSTEM DESCRIPTION

Scanning Tunneling Microscope (STM) and Atomic Force Microscope (AFM) were invented in 1980s. Both of them were a huge milestone on the history of nanoscience and nanotechnology. They enabled 3d-imaging of sample matter with atomic-scale precision. The STM was invented by Binning and Rohrer on 1981. STM uses a quantum-mechanical phenomenon of *tunneling current*, which is caused by flow of electrons from the surface of one material to another material when they are close to each other. However, STM can only work with conductive materials. In 1986, AFM was invented by Binning, Quate and Gerber. AFM uses a microscale cantilever probe, which is sensitive enough to deflect due to interaction forces between its tip and the atoms on the sample matter. Since the cantilever can detect interaction forces with any material, AFM can be used to image any material - not just electrically conducting materials[1]. A typical AFM setup is shown in Figure 2.1. Main components includes the cantilever beam, a laser, a photo diode, a dither piezo and an XYZ piezo-electric scanner.

2.1 AFM Components

2.1.1 Cantilever Beam

One of the most essential component on the AFM is the cantilever beam. The cantilever beam has a tip on it and as it is brought close to the sample, it feels the interaction forces between its tip atoms and the closest atoms on the sample surface. Due to this interaction forces, the cantilever deflects, which can be used to detect sample properties. Also since these interaction forces typically depend on the separation between the tip-atoms and the closest atoms on the sample, the cantilever deflections are used to determine sample profiles - thereby enabling sample imaging by moving the sample laterally under the cantilever. The forces between the cantilever tip and the the sample are usually in the range between $10^{-7} - 10^{-12}$ N, so the cantilevers need to be compliant enough to see some effects under this

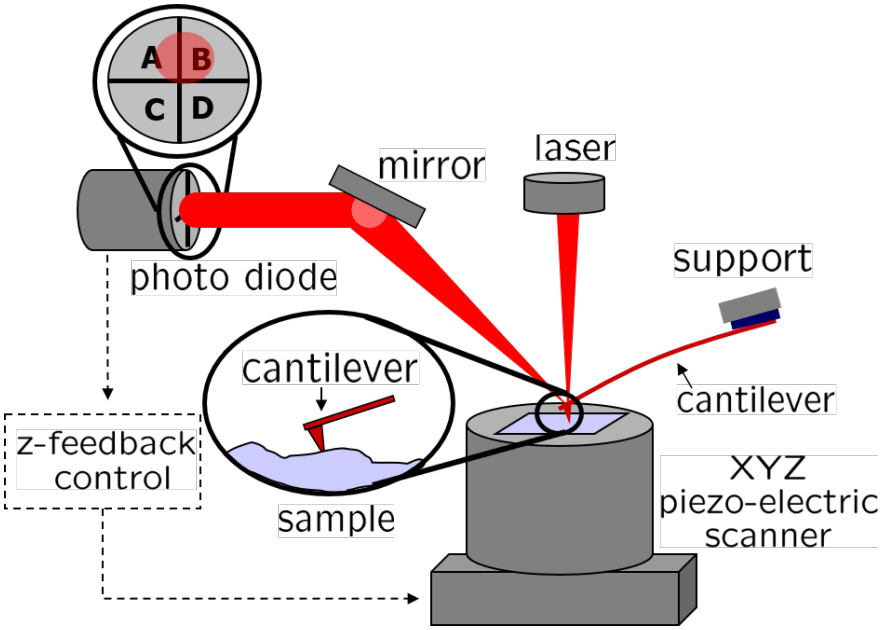

Figure 2.1: A diagram of atomic force microscope (AFM). Essential parts are shown here, including the cantilever beam, XYZ piezo-electric scanner, laser beam (working together with photo diode as sensor to sense the position of the cantilever beam), dither piezo (mounted on the cantilever support), and a z-feedback control usually exist depend on the design and use of the AFM [11]

amount of force. However, we also need to avoid external disturbances which are usually having power spectral density at lower frequencies. For example, building vibrations usually have power spectral density significant in $0-2$ kHz. As a result, the resonance frequency of the cantilever beam is always larger than 2 kHz. Typical length, width, and thickness of micro-cantilevers used in AFM are $100-300$, $30-40$, and $2-5$ μm respectively. Depending on the underlying applications, the stiffness of the micro-cantilever can vary from 0.06 to 100 N/m. The cantilever tip usually has tetrahedral or cone shapes, and the tip typically has radius about 5-10 nm[4]. In many situations, we want the AFM to run a "dynamic mode", where the cantilever beam is oscillating at an expected magnitude and frequency, so a *dither piezo* is usually mounted on the base (or support) of the cantilever beam to give a sinusoidal excitation and makes the cantilever oscillate at the expected frequency response.

2.1.2 Cantilever Beam Position Sensor

The laser beam and the photo diode is used to detect the position of the cantilever tip by shooting the laser beam at the top surface of the cantilever's free end. The cantilever beam is made that it can reflect the laser beam to the photo diode. As the cantilever

deflects due to its interaction with the sample, the position of the reflected laser spot on the photo-diode changes. This change in the position of the laser spot is measured by the photodiode as an electrical voltage signal. The changes in laser spot greatly amplify the changes in the cantilever tip position, especially when the reflected laser path is long. The term *Optical Lever Detection Sensitivity* (InvOLS) describes the optical sensor sensitivity. It is usually with a unit of nm/V, and describes how much voltage changes corresponding to how much cantilever beam deflection. Typical InvOLS are 1-100 nm/V[14]. Since the change of laser spot is indicative change of cantilever deflection, which itself is due to tip-sample interaction forces, this measurement can be used to estimate changes in tip-sample interaction forces. Since the changes in force primarily depend on the tip-sample separation distance, the photodiode signal can be calibrated to give a measurement of the tip-sample separation distance.

2.1.3 XYZ Piezo-electric Scanner

The XYZ piezo-electric scanner is used to change the relative positions of cantilever beam and sample laterally and vertically. The XY directions are used to move the sample laterally so the cantilever beam can scan an area of the sample. More precisely, since photodiode signal gives a measure of tip-sample separation distance, this signal when plotted against the XY coordinates gives a sample image over an area. The Z direction is used to adjust the distance between the cantilever beam and the sample. Different AFMs have different designs of XYZ piezo-electric scanner. Tube piezo-actuators generate XYZ motion by one piezoelectric cylinder; independent axis piezo-actuation separate the planar actuation and vertical actuation and can reduce the crosstalk between different moving directions. Set the XYZ scanner to move the cantilever and the optical base together or set the XYZ scanner to move the sample also result in different dynamic properties for the AFM[4].

2.2 Operation Modes

There are typically two categories of AFM operation modes: static mode and dynamic mode[1].

2.2.1 Static Mode Operation

For the static mode operation, the cantilever beam move horizontally through the sample without oscillation. Atomic interaction forces between the cantilever tip and the sample will give the cantilever beam different amount of deflection as the sample has different height along the scanning path. If no control system is used, we can look at the different deflection of the cantilever beam to find the sample topography. Since it is extremely difficult to maintain the lateral motion of the sample, which can be in hundreds of microns, within the separation range from the cantilever-tip where the tip-sample interaction forces are appreciable, it is practically infeasible to obtain sample-profiles directly from photodiode measurements. One method to resolve this problem is to apply a control system and run constant-force mode, where control system keeps the cantilever beam to be in constant deformation throughout the scanning process, by appropriately moving the sample in the vertical direction so as to compensate for the feature heights on the sample profile. In this mode, the control signal required to maintain a constant deflection is calibrated to provide the information of the sample profile. This implementation is still simpler when compared with dynamic mode operation of AFM, but this mode requires the cantilever beam to constantly apply forces to the sample, and large lateral forces are introduced as the cantilever scans laterally, this mode causes more tip damage and it is not preferred for soft samples such as biological tissues due to large shearing forces.

2.2.2 Dynamic Mode Operation

For the dynamic mode operation, the cantilever beam is actuated by the dither piezo on its base usually with a constant sinusoidal input, resulting in a harmonic oscillation. As the sample has different geometry below the cantilever beam, different atomic interaction forces will give the cantilever beam different frequency responses. Usually a control system is applied to keep the frequency responses same during the process, then the sample topography can be detected through signals in the control loop. When compared with static mode of operation, one big advantage is that the tip only taps the sample for short intervals during the scanning, the tip experiences less contact with sample and significantly smaller lateral forces. The tip will experience less wear, and the damage to the sample itself is also less, making the dynamic mode operation more preferable for biological tissues or other soft materials.

Figure 2.2 shows an experimental result of the effect of thermal noise and measurement noise measured by photo diode on the cantilever defection.[1] we can see measurement noise

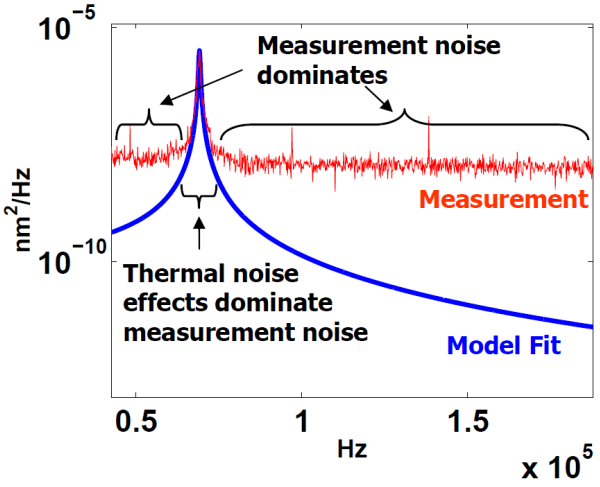

Figure 2.2: Effect of thermal noise and measurement noise on the cantilever deflection. The thermal noise effects dominate measurement noise around the natural frequency of the cantilever beam [1]

dominate thermal noise in most frequencies except that the thermal noises dominates around the resonance frequency. Around the resonance frequency, the measurement resolution is decided by thermal noise. When the signal of interest (say the cantilever deflection) is close to this frequency region, the signal-to-noise ratio (SNR) is very high, and limited only by the thermal noise. Thus during the dynamic mode operation of AFM, we drive the cantilever beam at a frequency close to the resonance frequency so we can benefit from higher SNR.

Dynamic mode operation AFM includes two main categories: amplitude modulation AFM (AM-AFM) and frequency modulation AFM (FM-AFM). As the sample interact with cantilever tip, the frequency response of the cantilever changes. Both the amplitude and the phase will change. AM-AFM uses a reference amplitude as control reference, and the controller will regulate the cantilever to maintain the amplitude at the reference. Comparing with FM-AFM, AM-AFM is more robust and more suited for samples with larger variance, and it can be better used for operation in fluid. Correspondingly, FM-AFM maintains the cantilever beam at a certain phase offset with the dither input. FM-AFM can use higher quality factor cantilever beam to achieve higher sensitivity at a higher bandwidth. However it is typically limited to be used under ultrahigh vacuum, low temperature conditions and for samples have small variation in topography. For this research we are focusing on the AM-AFM

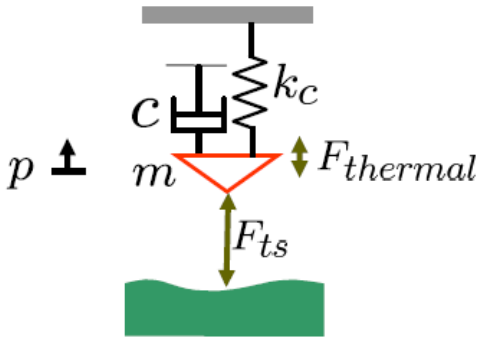

Figure 2.3: Diagram showing point mass model approximation of the cantilever beam [4]

2.3 Mathematical Model of Cantilever Beam

Using Euler-Bernoulli beam theory with assumption of small deflection of slender, uniform beam, and with boundary conditions that one end ($x = 0$) is clamped and the other end ($x = L$) is free, we can write the beam equation:

$$EI\frac{\partial^4}{\partial x^4}[\omega(x,t) + \gamma\frac{\partial\omega(x,t)}{\partial t}] + \mu\frac{\partial^2\omega(x,t)}{\partial t^2} = F(x,t) \tag{2.1}$$

where x is the coordinate along the beam, $\omega(x,t)$ is the dynamic deflection at coordinate x and time t, E is the Young's modulus, I is the moment of inertia, μ is the linear mass density, γ is the internal damping coefficient of the beam and $F(x,t)$ is the force acting on the cantilever.

To simplify the physical model shown by Equation 2.1, a point mass model like Figure 2.3 can be used if we mostly care about the first mode of the cantilever beam. Although under the effect of tip-sample interaction force, frequency responses at higher harmonics show different properties for beams and point masses, in the air ($Q \sim 100 - 1000$) and large first mode frequency ($f_0 \geq 10^5$), magnitude of the higher harmonic responses are about three orders of magnitude smaller than the fundamental frequency. As a result, for a cantilever beam operating in air or vacuum (high quality factor Q situations), we can usually simplify the model represented by Equation 2.1 with the following point mass model[5]

$$\ddot{p} + 2\frac{\omega_0}{Q}\dot{p} + \omega_0^2 p = \frac{1}{m_e}(F_{dither} + F_{ts} + F_{thermal}) \tag{2.2}$$

where p is the position of the cantilever tip, ω_0 is the first modal frequency, and m_e is the effective mass of the cantilever and the tip, Q is the quality factor which is related with the

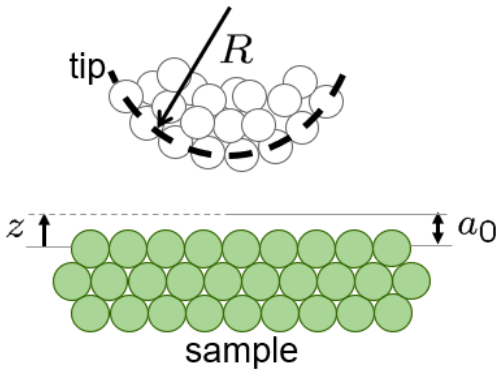

Figure 2.4: The diagram of the physical model used to estimate the DMT model of tip-sample interation[11]

damping. Q is usually up to 10 in liquid, 100 to 500 in air, and 10,000 or higher in vacuum. F_{dither} is the force from dither piezo, F_{ts} is the tip-sample interaction force, $F_{thermal}$ is the thermal noise. $F_{dither} + F_{ts} + F_{thermal}$ represent the main components of the external forcing in Equation 2.1.

2.4 Tip-Sample Interaction Models

For AFM studies, one prevalent model to describe the force between cantilever tip and the sample is Derjaguin-Müller-Toporov (DMT) model. DMT model includes the effect of Van der Waals force between atoms and Hertz model contacting, and it is based on approximating the physical setup as the setup shown in Figure 2.4. Hertz model helps describing the repulsive force during the contact, and this repulsive force are larger in magnitude while effcting in a shorter distance. Van der Waals force gives attraction forces in a longer range, but the magnitude of the attraction force is smaller and dominated by repulsive forces at short distances. DMT model is usually applied to tips with small curvature radius and high stiffness under dry conditions[2][4]. For this study DMT model is used to model the tip-sample interaction forces in the simulation. DMT model is given by equations:

$$F_{ts}(z) = \begin{cases} -\dfrac{HR}{6z^2}, & \text{if } z > a_0 \\ -\dfrac{HR}{6a_0^2} + \dfrac{3}{4}E^*\sqrt{R}(a_0 - z)^{\frac{3}{2}}, & \text{if } z \leq a_0 \end{cases} \tag{2.3}$$

where H is the Hamaker constant (a material constant), R is the tip radius, E^* is the effective Young's modulus, a_0 is the intermolecular distance, z is the distance between tip and sample.

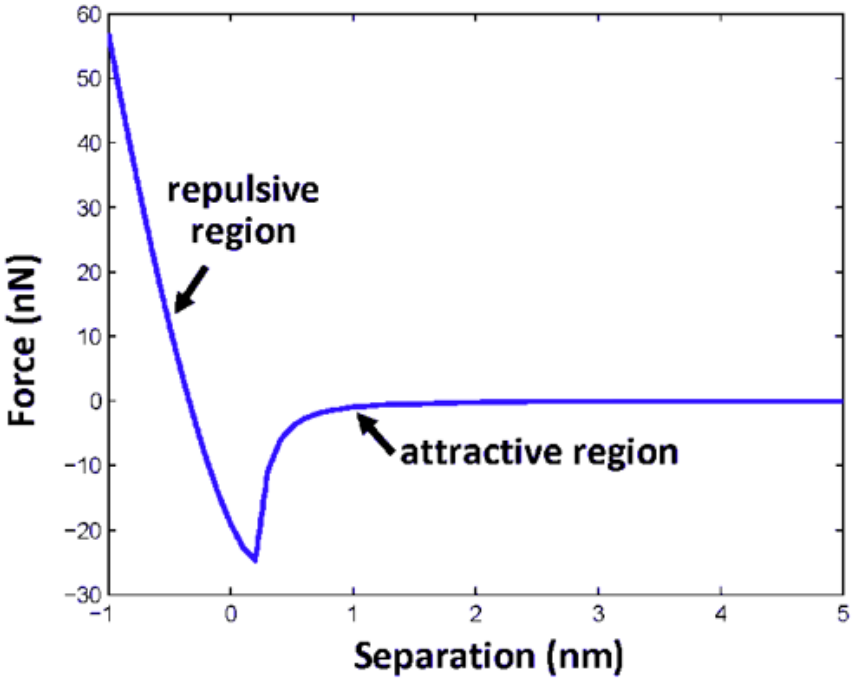

Figure 2.5: A general example of how the atomic interation forces between cantilever tip and samples estimated by DMT method might look like. The right side shows the long range attractive forces, and the left side shows the repulsive forces experiences by the tip when they are closer to the sample [11]

The effective Young's modulus is affected by both the tip material and the sample material, and is given by equation:

$$\frac{1}{E^*} = \frac{1-\nu_{tip}^2}{E_{tip}} + \frac{1-\nu_{sample}^2}{E_{sample}} \tag{2.4}$$

An example of the force vs tip-sample distance relationship under DMT model is given in the Figure 2.5.

CHAPTER 3

DIRECT-QUADRATURE-FRAME TRANSFORMATION AND SIMULATION RESULTS

3.1 Direct-Quadrature (DQ) Transformation

The direct-quadrature (dq) transformation represents a transformation of two-dimensional vectors in a static reference frame to a rotating frame. Often the two dimensional vectors are represented by complex numbers in a complex plane. The dq transform is often used in the context of electrical engineering with three-phase circuits. The transform can be used to rotate the reference frames of ac waveforms such that they become dc signals.

Nearly harmonic signals of the form $A(t)\sin(\theta(t))$ can be represented as complex functions or *phasors* where the magnitude and angle of the complex numbers are amplitude $A(t)$ and $\theta(t)$ respectively. For example, for constant amplitude and frequency $\omega = \dfrac{d\theta}{dt}$, the complex number $f(t)$ traverses a circle (a rotating phasor) on the complex plane with radius A and the frequency of oscillations is ω. The rectangular (cartesian-coordinate) frame is referred to as $\alpha\beta$ frame, where the real and imaginary parts of the fixed complex plane are the α and the β axes. Here the α and β coordinates of a rotating phasor are themselves harmonic signals $A\cos(\omega t + \phi)$ and $A\sin(\omega t + \phi)$ respectively. The rotating phasor in this fixed frame is accordingly given by $f_{\alpha\beta}(t) = Ae^{j(\omega t+\phi)}$. In power systems, most signals are oscillating at a certain frequency, [12] shows a typical example where we can look at the system in dq-frame and control it. The following control design can focus on regulate low frequency signals instead of designing the control at the frequency where the signals are oscillating at, which is usually more difficult.

The dq reference frame corresponds to a rotating axes system to describe complex numbers, where the real and imaginary axes are rotating with a specified frequency ω. Figure 3.1 shows a diagram of the rotating phasor in $\alpha\beta$-frame and dq-frame. Given the phasor $\vec{f}$ that is represented in the $\alpha\beta$-frame as:

$$\vec{f}_{\alpha\beta} = f_\alpha + jf_\beta = Ae^{j\theta(t)} \tag{3.1}$$

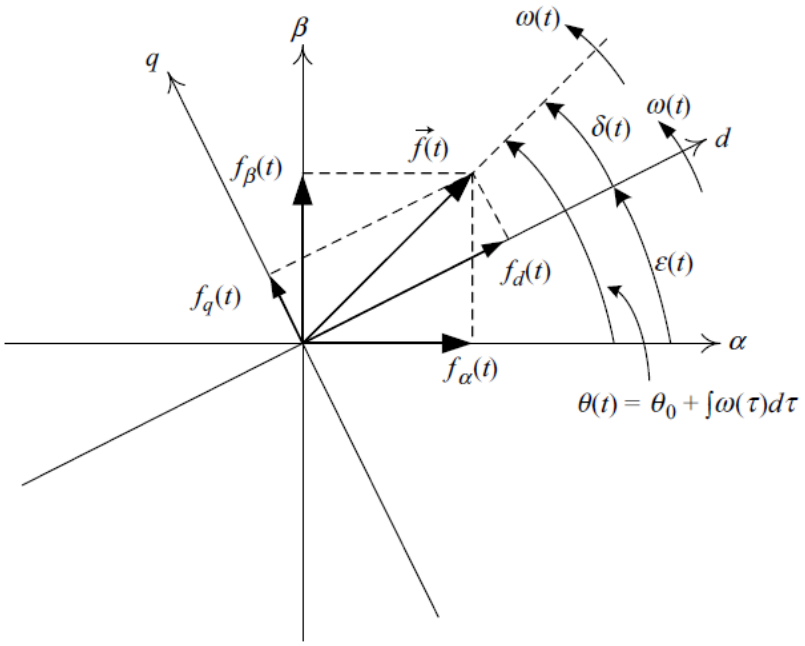

Figure 3.1: Representation of a space phasor in $\alpha\beta$-frame and dq-frame. $\alpha\beta$-frame is a steady frame, while dq-frame is a rotating frame, but it is relatively steady to the phasor $\vec{f}$ [9]

this phasor is represented in the dq-frame by:

$$\vec{f}_{dq} = f_d + jf_q = (f_\alpha + jf_\beta)e^{-j\varepsilon(t)} = Ae^{j(\theta(t)-\varepsilon(t))} \tag{3.2}$$

where $\varepsilon(t)$ is the angle shift from $\alpha\beta$-frame to dq-frame. In this coordinate system, the rotating phasor $f_{\alpha\beta}(t) = Ae^{j(\omega t+\phi)}$ is represented by a *static* phasor $f_{dq}(t) = Ae^{j\phi}$. In the dq-frame, the phasor is steady, and the projection of the phasor on the d-axis and q-axis better represents amplitude and phase, which both are constant values as the signal is oscillating harmonically. In general, phasors $f_{\alpha\beta}(t)$ in $\alpha\beta$ system transform to $f_{dq} = f_{\alpha\beta}e^{-j\omega t}$ in the dq system.

Because during the dynamic mode operation of AFM, the cantilever beam is under a forced oscillation drived by the dither piezo, it is oscillating close to the input frequency, the dq-frame is applied on the AFM to find a expression of the amplitude and phase of the cantilever beam.

To find a mathematical model for the amplitude and phase of the AFM, we start with Equation 2.2. Equation $Q = \frac{1}{2\zeta}$ is used to bring in damping coefficient ζ to the equation. In this thesis, we are interested in obtaining the open-loop model, therefore no feedback control

is assumed; also we consider the tip-sample interaction force depend on $p-h$, where the effect of the sample vertical motions q are not explicitly considered since $q+h$ can be replaced by only h without any loss of generality. Thermal noise $F_{thermal}$ is also not considered for the input force now. An simplified AFM system for the following analysis can be expressed as:

$$\ddot{p} + 2\zeta\omega_n\dot{p} + \omega_n^2 p = \frac{1}{m_e}(F_{dither} + F_{ts}(p-h)) \tag{3.3}$$

where p is the position of the cantilever beam, ζ is the damping, ω_n is the natural frequency, F_{dither} is the input from dither that drives the cantilever beam oscillation, h is the height of the sample, F_{ts} is the interaction force between cantilever beam tip and the sample and it is a function of the distance between cantilever beam position and sample height $p-h$, m_e is the equivalent mass for the cantilever beam. In the following equations, we use a function $g(x)$ to express the tip-sample interaction force, where:

$$g(x) = \frac{1}{m_e}F_{ts}(x) \tag{3.4}$$

Since we are giving constant harmonic inputs to the cantilever beam, dither input can be expressed as:

$$\frac{1}{m_e}F_{dither} = \sigma\cos(\omega t). \tag{3.5}$$

We view the system in Equation 3.3 as the an α component of a phasor, where the β component is a *fictitious* cantilever system that we design - which has same material properties except that it is forces by a dither signal and a tip-sample interaction signal, which is $\frac{\pi}{2}$ radians (a quarter period) out of phase with that of the real (α-component) system. that is,

$$\begin{cases} \ddot{p}_\alpha + 2\zeta\omega_n\dot{p}_\alpha + \omega_n^2 p_\alpha = \sigma\cos(\omega t) + g(p_\alpha - h(t)) \\ \ddot{p}_\beta + 2\zeta\omega_n\dot{p}_\beta + \omega_n^2 p_\beta = \sigma\sin(\omega t) + g(p_\beta - h(t-\frac{T}{4})) \end{cases} \tag{3.6}$$

where $T = \frac{2\pi}{\omega}$ is the time for one period.

We consider the rotating phasor $p_{\alpha\beta} = p_\alpha + jp_\beta$, and introduce the dq coordinate transformation:

$$p_{\alpha\beta} = p_{dq}e^{j\omega t+\phi_g} \tag{3.7}$$

Therefore $p_{\alpha\beta}$, $\dot{p}_{\alpha\beta}$ and $\ddot{p}_{\alpha\beta}$ are given by:

$$\begin{cases} p_{\alpha\beta} = p_{dq}e^{j\omega t+\phi_g} \\ \dot{p}_{\alpha\beta} = \dot{p}_{dq}e^{j\omega t+\phi_g} + j\omega p_{dq}e^{j\omega t+\phi_g} \\ \ddot{p}_{\alpha\beta} = \ddot{p}_{dq}e^{j\omega t+\phi_g} + 2j\omega\dot{p}_{dq}e^{j\omega t+\phi_g} - \omega^2 p_{dq}e^{j\omega t+\phi_g} \end{cases} \tag{3.8}$$

On substituting Equation 3.8 into Equation 3.6, we get:

$$\begin{aligned}(\ddot{p}_{dq} + 2j\omega\dot{p}_{dq} - \omega^2 p_{dq})e^{j\omega t+\phi_g} + 2\zeta\omega_n(\dot{p}_{dq} + j\omega p_{dq})e^{j\omega t+\phi_g} + \omega_n^2 p_{dq}e^{j\omega t+\phi_g} \\ = \sigma e^{j\omega t} + g_{dq}(p_\alpha - h(t), p_\beta - h(t-\frac{T}{4}))e^{j\omega t+\phi_g}\end{aligned} \tag{3.9}$$

where $g_{dq}e^{j\omega t+\phi_g}$ represents the tip sample interaction force went through the coordinate transformation.

When we divide two sides of the Equation 3.9 by $e^{j\omega t+\phi_g}$ and use relationship: $p_{dq} = p_d + jp_q$, we obtain the AFM dynamics under dq-coordinates:

$$\begin{cases} \ddot{p}_d + 2\zeta\omega_n\dot{p}_d - 2\omega\dot{p}_q + (\omega_n^2 - \omega^2)p_d - 2\zeta\omega_n\omega p_q = \sigma\cos(-j\phi_g) + g_d \\ \ddot{p}_q + 2\zeta\omega_n\dot{p}_q + 2\omega\dot{p}_d + (\omega_n^2 - \omega^2)p_q + 2\zeta\omega_n\omega p_d = \sigma\sin(-j\phi_g) + g_q \end{cases} \tag{3.10}$$

where g_d and g_q are both functions of $(p_\alpha - h(t))$ and $(p_\beta - h(t - \frac{T}{4}))$

We rewrite Equation 3.10 in matrix form:

$$\begin{pmatrix}\ddot{p}_d \\ \ddot{p}_q\end{pmatrix} + 2\begin{pmatrix}\zeta\omega_n & -\omega \\ \omega & \zeta\omega_n\end{pmatrix}\begin{pmatrix}\dot{p}_d \\ \dot{p}_q\end{pmatrix} + \begin{pmatrix}\omega_n^2 - \omega^2 & -2\zeta\omega_n\omega \\ 2\zeta\omega_n\omega & \omega_n^2 - \omega^2\end{pmatrix}\begin{pmatrix}p_d \\ p_q\end{pmatrix} = \begin{pmatrix}\sigma\cos(-\phi_g) + g_d \\ \sigma\sin(-\phi_g) + g_q\end{pmatrix}. \tag{3.11}$$

The analysis of the above equations is given by interpreting Equation 3.6. Note that since the cantilever model is causal, and the inputs to the real cantilever (the α-component) and the fictitious cantilever (β-component) are the same except that there is a phase difference of $\frac{\pi}{4}$ between them, the solutions for p_α and p_β are expected to be identical except that they are $\frac{\pi}{4}$ radians apart in phase; that is p_β lags behind p_α by $T/4 = \frac{2\pi}{4\omega}$. We view p_α and p_β as the real and imaginary part of a rotating phasor $\vec{p}_{\alpha\beta}$. This rotating phasor represents the oscillation of the cantilever beam. After the coordinate transformation, phasor $\vec{p}_{dq}$ is a static phasor in the rotating dq-coordinate plane. If ϕ_g is chosen that it equals the phase difference between the dither input and the cantilever beam oscillation, $\vec{p}_{dq}$ will align with the x axis, in which case, p_d represents the oscillation magnitude, and the fictitious component p_q is zero. .

3.2 KBM Model

During a cantilever beam oscillation process, the attractive force is in effect for a longer distance but it is small, and the repulsive force is larger but it is only in effect for a short distance. We can use asymptotic perturbation methods on this type of weak nonlinear system. The Krylov-Bogoliubov-Mitropolskii (KBM) method can be applied on the system expressed by Equation 2.2. Give the Equation 2.2 a more detailed expression with sample height and control effort added as varables:

$$\ddot{p} + 2\frac{\omega_0}{Q}\dot{p} + \omega_0^2(p - v) = \frac{1}{m_e}(F_{dither} + F_{ts}(p - h) + F_{thermal}) \tag{3.12}$$

where h is the sample height, v is the control input represents an actuator mounted on the cantilever beam base and controls the Z-axis movement. Alternatively, if the control input v is installed under the sample, Equation 2.2 will be expressed as:

$$\ddot{p} + 2\frac{\omega_0}{Q}\dot{p} + \omega_0^2 p = \frac{1}{m_e}(F_{dither} + F_{ts}(p - h - v) + F_{thermal}) \tag{3.13}$$

Process Equation 3.12 with KBM method, we can get equations describe the dynamics of oscillation amplitude and phase:

$$\begin{cases} \dfrac{dA}{dt} = -\zeta\omega_0 A - \dfrac{\omega_0^2 g_0}{2\omega}\sin\phi \\ \dfrac{d\phi}{dt} = \omega_0 - \omega - \dfrac{1}{2\pi\omega A}\displaystyle\int_0^{2\pi} \frac{1}{m} F_{ts}(A\cos\theta - h + v)\cos\theta\, d\theta - \frac{\omega_0^2 g_0}{2\omega A}\cos\phi \end{cases} \tag{3.14}$$

where ω is the frequency of the dither input, h is the sample height, and v is the actuator input. Again, in the case of control input under the sample with Equation 3.13, the AFM model processed by KBM method can be expressed as:

$$\begin{cases} \dfrac{dA}{dt} = -\zeta\omega_0 A - \dfrac{\omega_0^2 g_0}{2\omega}\sin\phi \\ \dfrac{d\phi}{dt} = -\omega_0 - \omega - \dfrac{1}{2\pi\omega A}\displaystyle\int_0^{2\pi} \frac{1}{m} F_{ts}(A\cos\theta - h - v)\cos\theta\, d\theta - \frac{\omega_0^2 g_0}{2\omega A}\cos\phi \end{cases} \tag{3.15}$$

Although KBM method gives equations for the dynamics of amplitude and phase, this method assumes slow varying h and v. In [4], a sinusoidal sample profile h with amplitude 10 nm and frequency 100 Hz and another sinusoidal h with amplitude 10 nm and frequency 2500 Hz are tested for the KBM method. Results from KBM method and result from the simulation of the physical model itself (represented by Equation 3.12) are compared, results

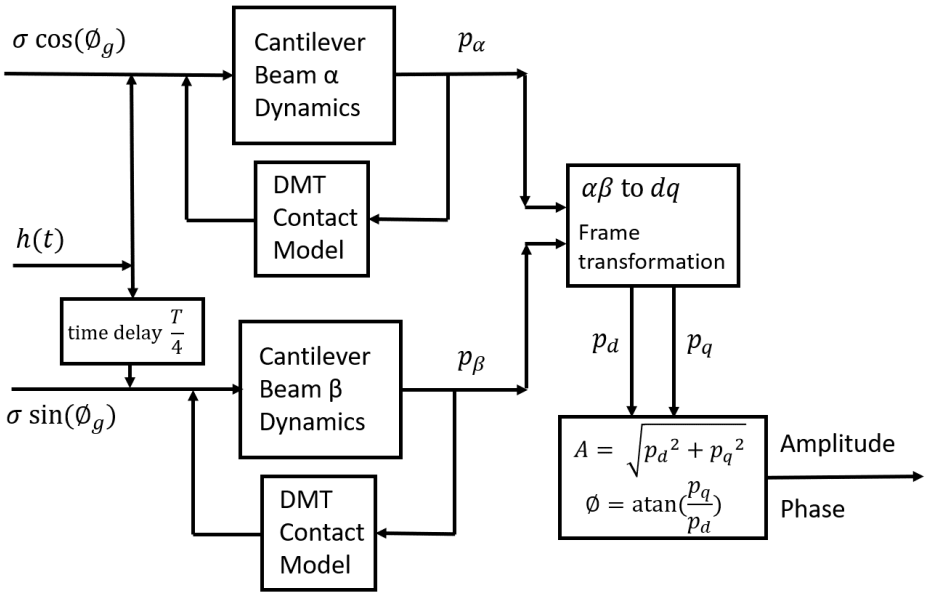

Figure 3.2: Block diagram of the Simulink simulation setup

shows that when h has a frequency of 100 Hz, the dynamics are following well, but it goes significantly off at the frequency of 2500 Hz.

3.3 Simulation Results with Proposed Model

To simulate the performance of dq coordinate transformation, a simulation of the physical system based on Equation 3.6 is implemented in the Simulink, and the corresponding dq-coordinate transformation represented by Equation 3.7 is implemented to observe the dynamics under dq-coordinates. Also, the tip sample interaction forces are simulated with DMT model described by Equation 2.3. The structure of the simulation setup is shown in Figure 3.2. Figure 3.3 shows how the cantilever beam and sample feature are placed for the simulation. The properties of a Olympus AC240TS cantilever is used for the cantilever beam dynamics, with quality factor $Q = 158.5$, stiffness $k = 1.99$ N/m, first modal frequency $f_0 = 75.731$ kHz. The bode plot of the cantilever beam with the given parameters are given by Figure 3.4. To simulate the DMT model of tip-sample interaction forces, additional parameters are used: the Hamaker constant $H = 6.4 \times 10^{-20}$ J, the tip radius $R = 10.0 \times 10^{-9}$ m, the effective Young's modulus $E^* = 50.0 \times 10^9$ Pa, the intermolecular distance $a_0 = 0.16 \times 10^{-9}$ m [4]. The DMT model with the given parameters are shown by Figure 3.5. Respectively, the bode plot of the system described by dq-frame is given by

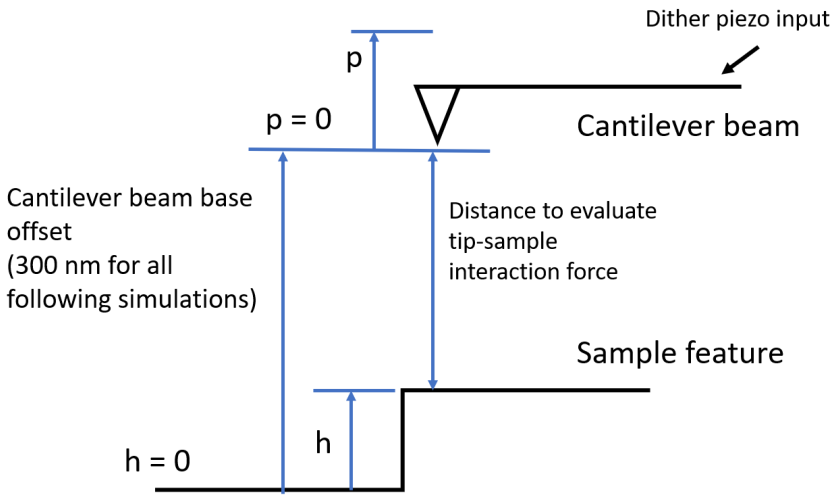

Figure 3.3: Diagram showing cantilever beam and sample feature setups in the simulation

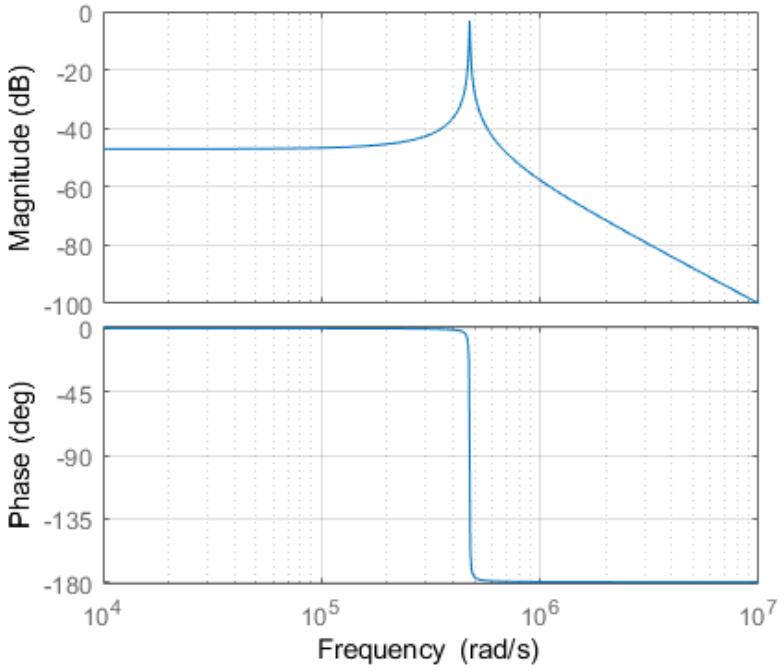

Figure 3.4: Bode diagram of the cantilever beam with given parameters (magnitude in nm)

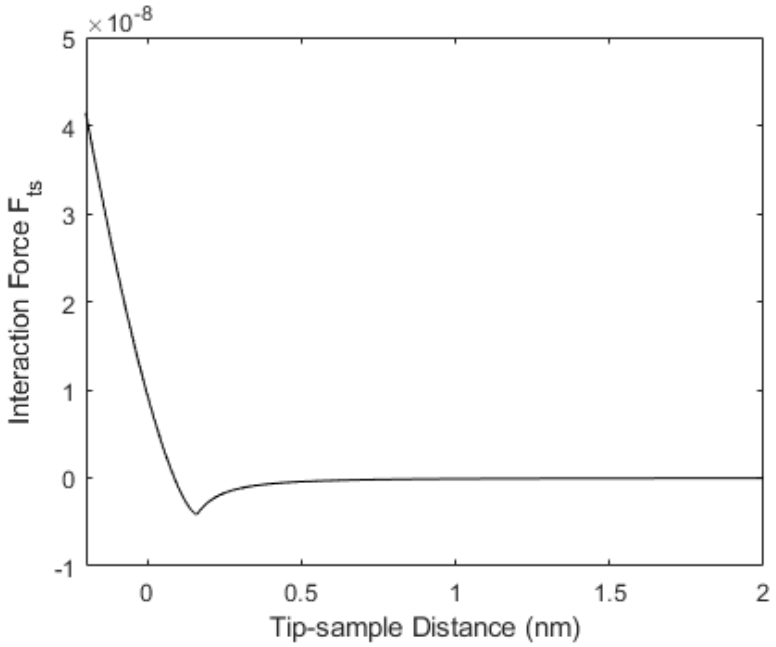

Figure 3.5: DMT model with given parameters

Figure 3.6. Comparing with Figure 3.4, where the peak is at f_0, the bode plot shown by Figure 3.6 has its "peak'moved to the low frequency range. However, the peak at frequency close to $2f_0$ rises possible concerns.

3.3.1 Oscillation in Air and Constant Heights

To verify the simulation and the dq-frame transformation on the most basic perspective, a pure cantilever beam oscillation without tip-sample interaction forces are tested. The inputs are set to make the cantilever beam has a free-air magnitude of 300 nm, and the driving frequency is at 95% target percent (the frequency response of Equation 2.2 has 95% of the magnitude at resonance frequency), resulting in a driving frequency of 75.651 kHz. Figure 3.7 shows the result of this basic simulation as expected. The cantilever beam is oscillating at a constant magnitude of 300 nm. The amplitude and phase calculated from $\vec{p}_{dq}$ are constant, and the amplitude calculated by dq-frame, $|\vec{p}_{dq}|$ are matching the 300 nm magnitude closely.

In addition, the performance of the dq-frame is tested under a constant height input. The base of the cantilever beam is set at 300 nm above the zero height reference, and a constant height of 20 nm is fed into the system. Figure 3.8 shows the result under the constant height, and the amplitude signal is following the constant amplitude of p_α closely as expected.

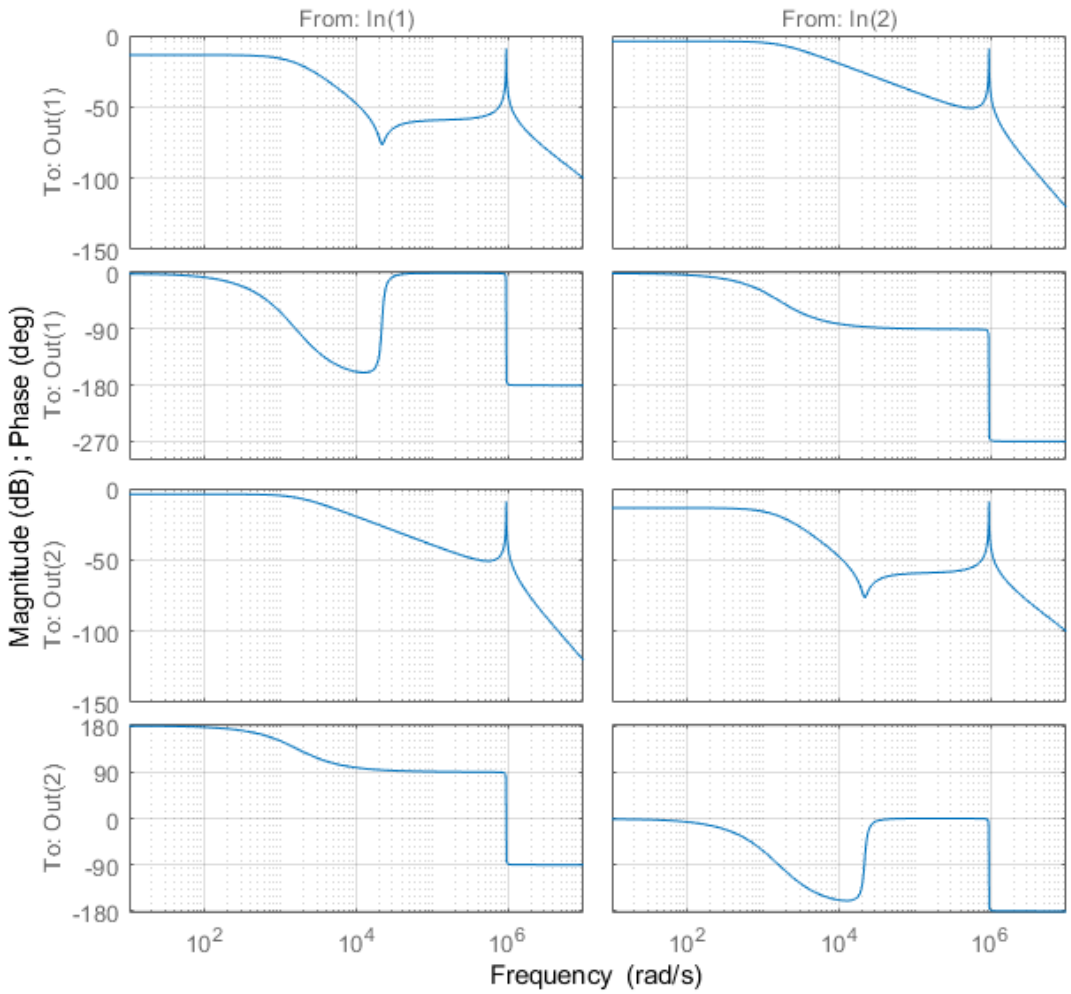

Figure 3.6: Bode plot of the system after dq-frame transformation, represented by Equation 3.11. The response has its maximum at low frequency range. However, a new peak at frequency close to $2f_0$ appears.

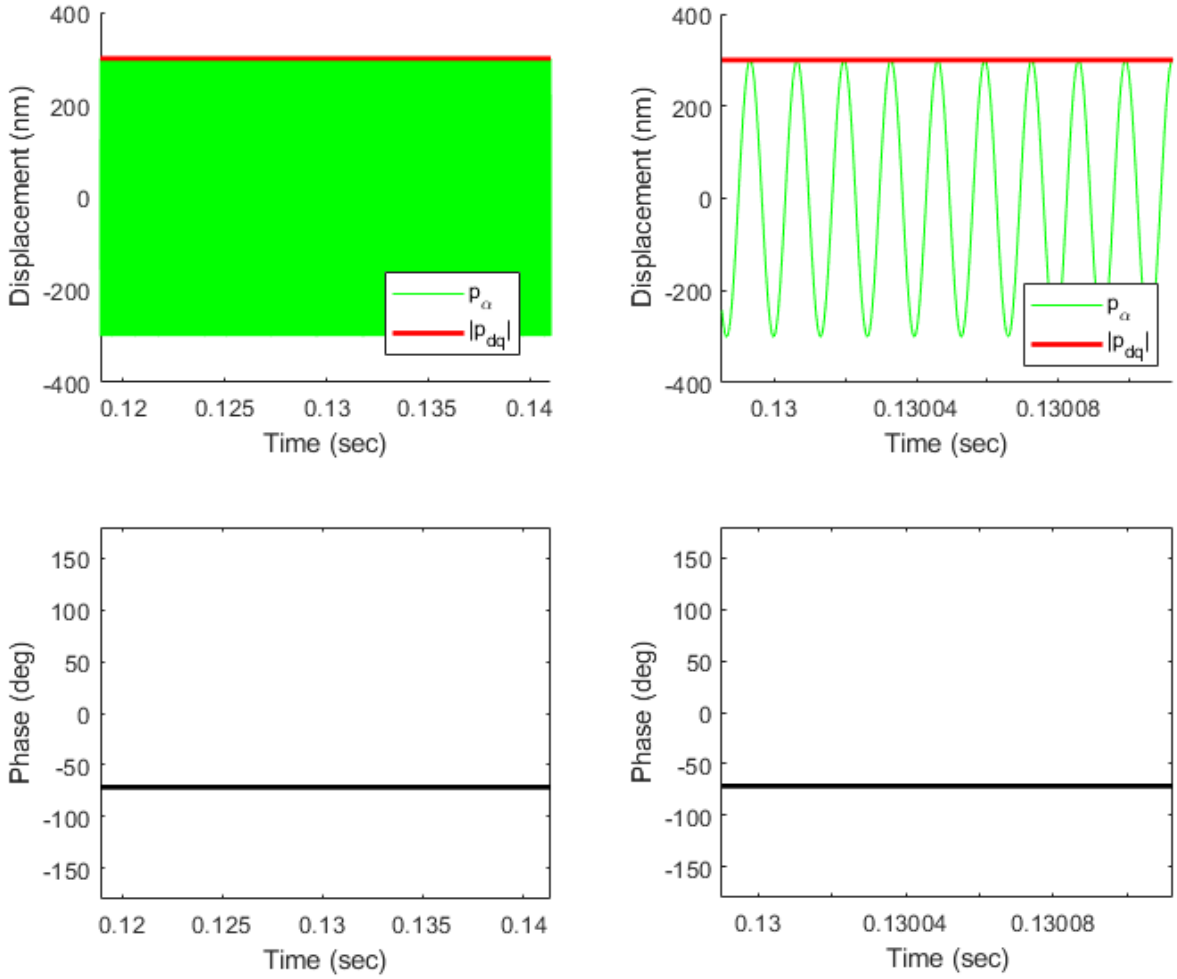

(a) general view

(b) zoomed-in view

Figure 3.7: Simulation results with no tip-sample interaction forces

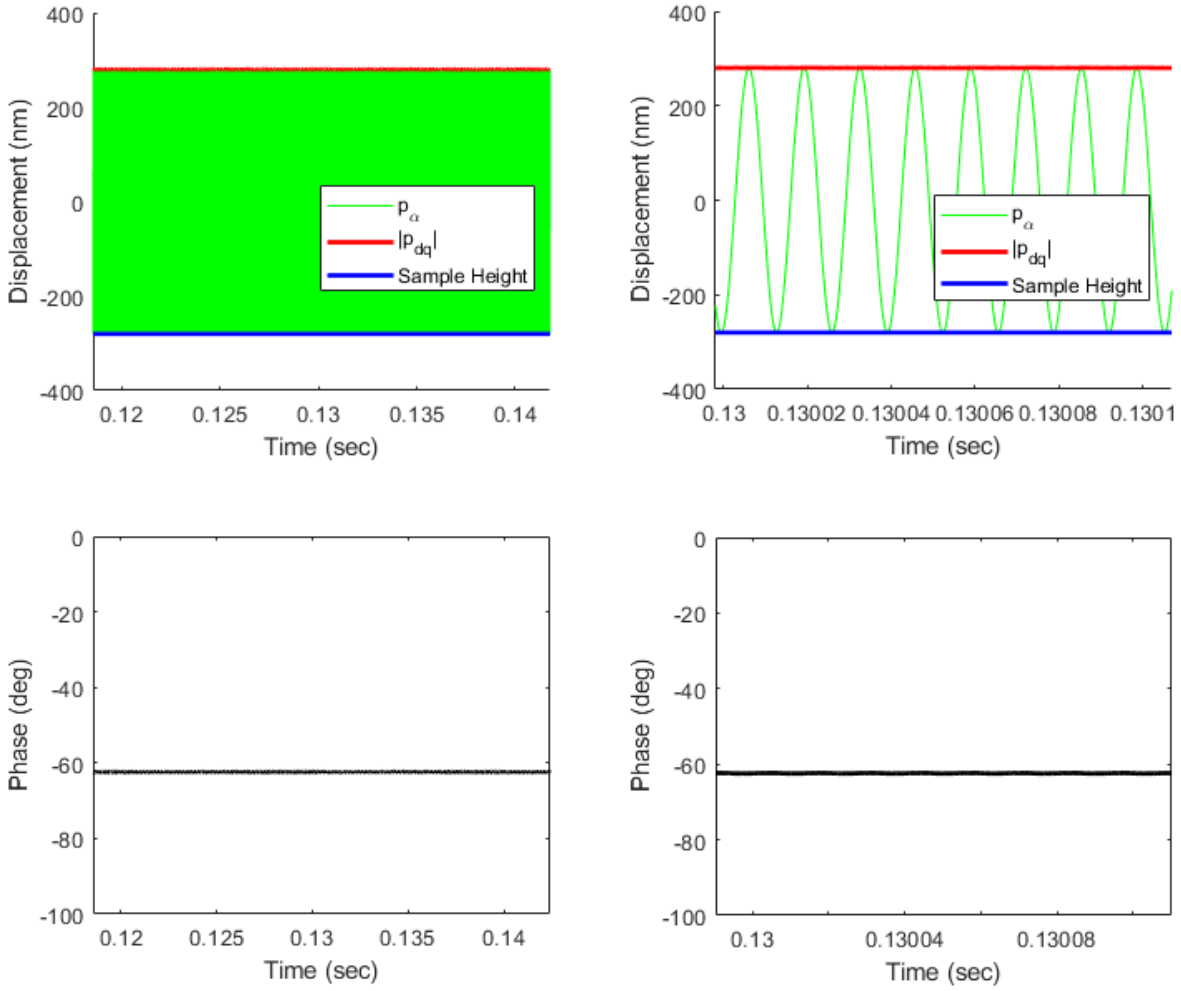

(a) general view

(b) zoomed-in view

Figure 3.8: Simulation results with constant height of 20 nm fed into the system

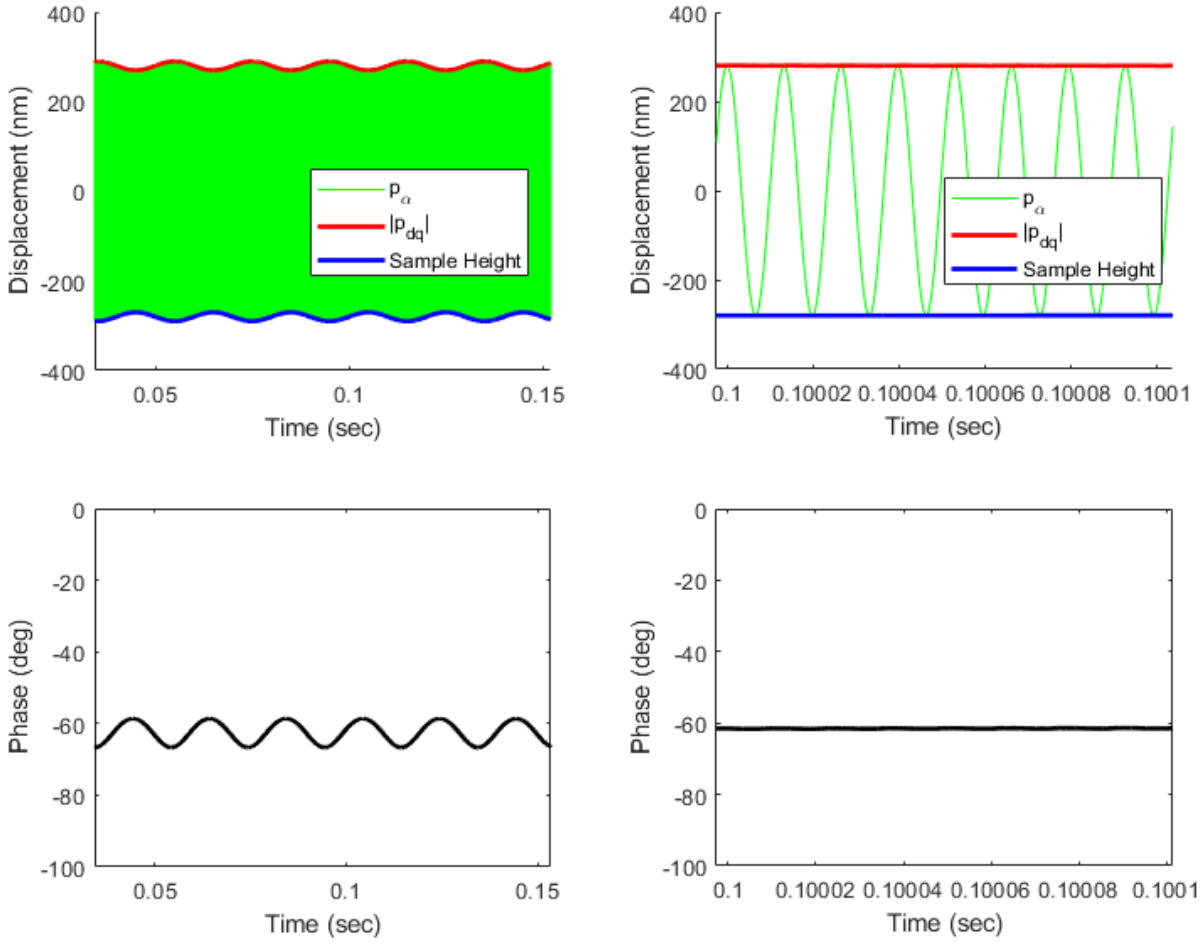

(a) general view

(b) zoomed-in view

Figure 3.9: Simulation results with heights oscillating between 10 nm and 30 nm at 100 Hz

3.3.2 Oscillation with Sinusoidal Heights

To test the performance of describing the system in dq-frame, varying heights are simulated under the cantilever beam and the system output after dq-frame transformation are observed. In all following simulations, the dither input is set that the cantilever beam has a free-air magnitude of 300 nm, and the driving frequency is at 75.651 kHz. Again, the base of the cantilever beam is set at 300 nm above the zero height reference.

Figure 3.9 shows the simulation result when a sinusoidal height oscillating between 10 nm and 30 nm at 100 Hz is fed into the system. The amplitude calculated by the dq-frame is following p_α closely as expected.

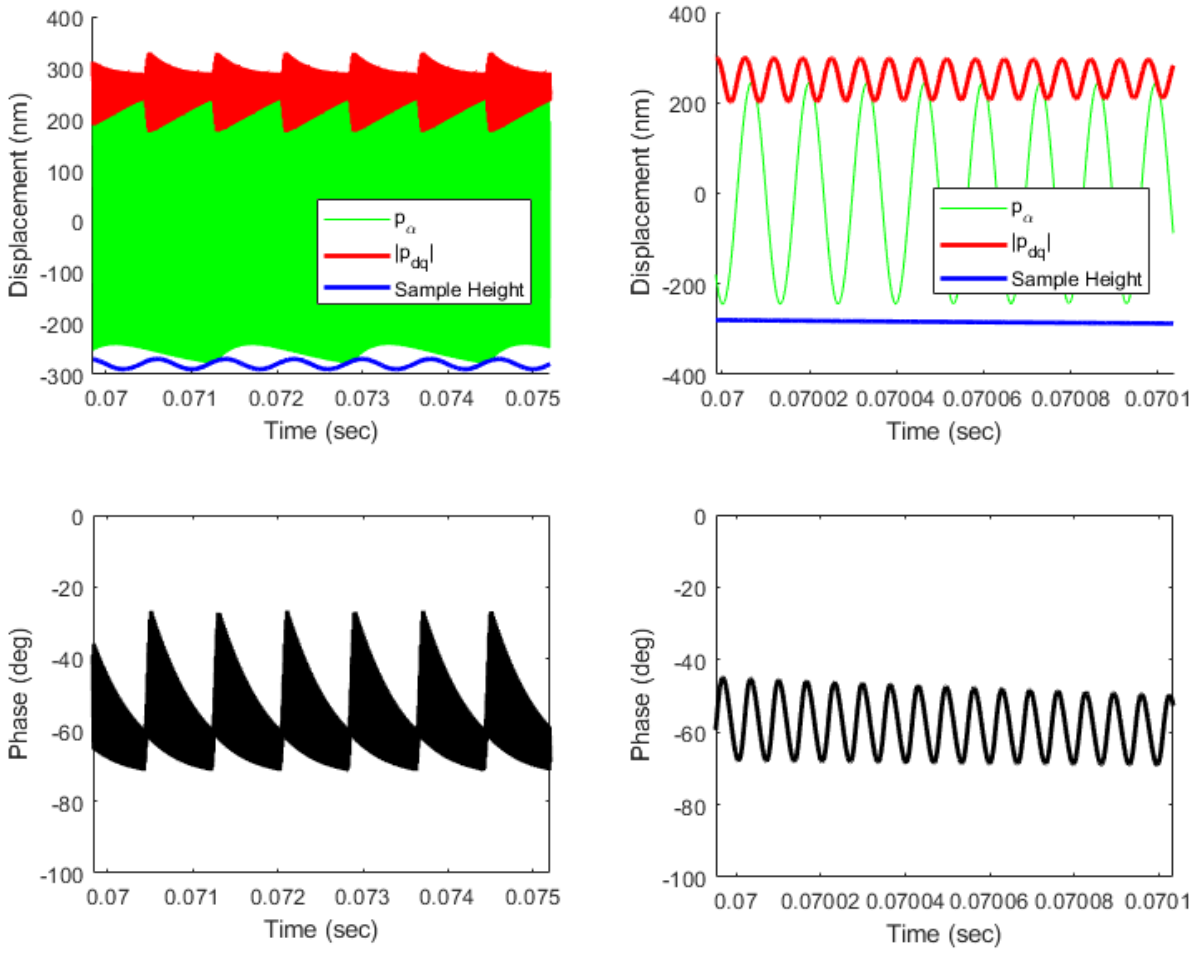

(a) general view

(b) zoomed-in view

Figure 3.10: Simulation results with heights oscillating between 10 nm and 30 nm at 2500 Hz

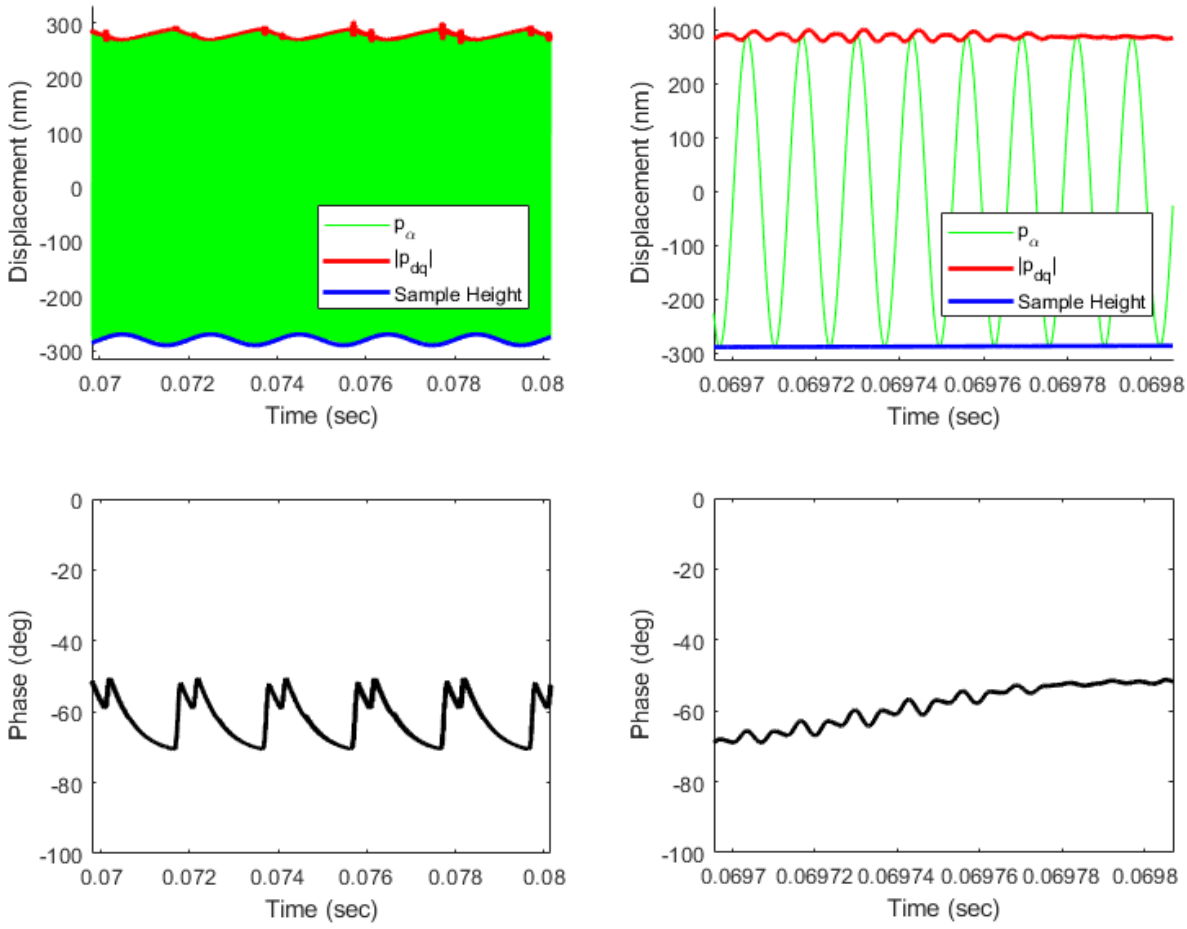

(a) general view

(b) zoomed-in view

Figure 3.11: Simulation results with heights oscillating between 10 nm and 30 nm at 1000 Hz

Figure 3.10 shows the simulation result when a sinusoidal height oscillating between 10 nm and 30 nm at 2500 Hz is fed into the system. The amplitude and phase calculated by the dq-frame goes significantly off comparing with p_α. Taking a closer look to the amplitude and phase, high frequency oscillations with approximately 2 times of the input frequency are dominating the signals.

As a result, this model describing amplitude and phase is working better when the amplitude and phase are affected by heights less than 2 kHz. Figure 3.11 shows the performance when a sinusoidal height oscillating between 10 nm and 30 nm at 1000 Hz is fed into the system. The amplitude signal is still following the profile of p_α closely although a little bit

high frequency components exist.

3.3.3 Notch Filter

In Figures 3.10 and 3.11, the amplitude and phase signals are disturbed by extra high frequency components. They are having a frequency close to 2 times the input frequency. The bode plot given by Figure 3.6 shows the system transfer function of the linear system on the left side of the Equation 3.11. The peak on the right side of each magnitude response plots shows that there is a peak at about two times of the input frequency. A notch filter could be connected before the output to counteract this peak and make the resulting system closer to the actual magnitude.

The following notch filter is connected at the amplitude and phase output, as it is shown in the block diagram Figure 3.13:

$$H = \frac{s^2 + 1901s + 9.036 \times 10^{11}}{s^2 + 9.506 \times 10^5 s + 9.036 \times 10^{11}} \tag{3.16}$$

and Figure 3.12 shows the bode plot of the system represented by Equation 3.11 filtered by H. In the simulation, filter H is connected at the amplitude and phase output.

Figure 3.14 shows the simulation result when a sinusoidal height oscillating between 10 nm and 30 nm at 1000 Hz is fed into the system, and the filter H is connected at the output, and Figure 3.16 shows the simulation result when a sinusoidal height oscillating between 10 nm and 30 nm at 2500 Hz is fed into the system, and the filter H is connected at the output. From Figure 3.14 we can see the high frequency components of amplitude and phase are mostly eliminated. Figure 3.15 offers a close-in comparison of filtered model and unfiltered model. Result shows that the filtered model can reduce the high frequency component to less than 16% of the original amount, giving a amplitude profile a lot closer to the actual amplitude. However, as we can see from Figure 3.16, even if the filter is applied and the oscillations at 2 times the driving frequency are mostly filtered, the amplitude is not matching the profile of p_α very well, and the amplitude signal is still containing oscillations at about 5 times of the driving frequency. Thus the filtered system is still only working well under 2 kHz, but it is closer to the actual amplitude compared with the unfiltered system. For the purpose of control design, instead of only using the system transfer function G derived from Equation 3.11, system HG will offer a better estimation of the amplitude and phase dynamics within the working range of this model.

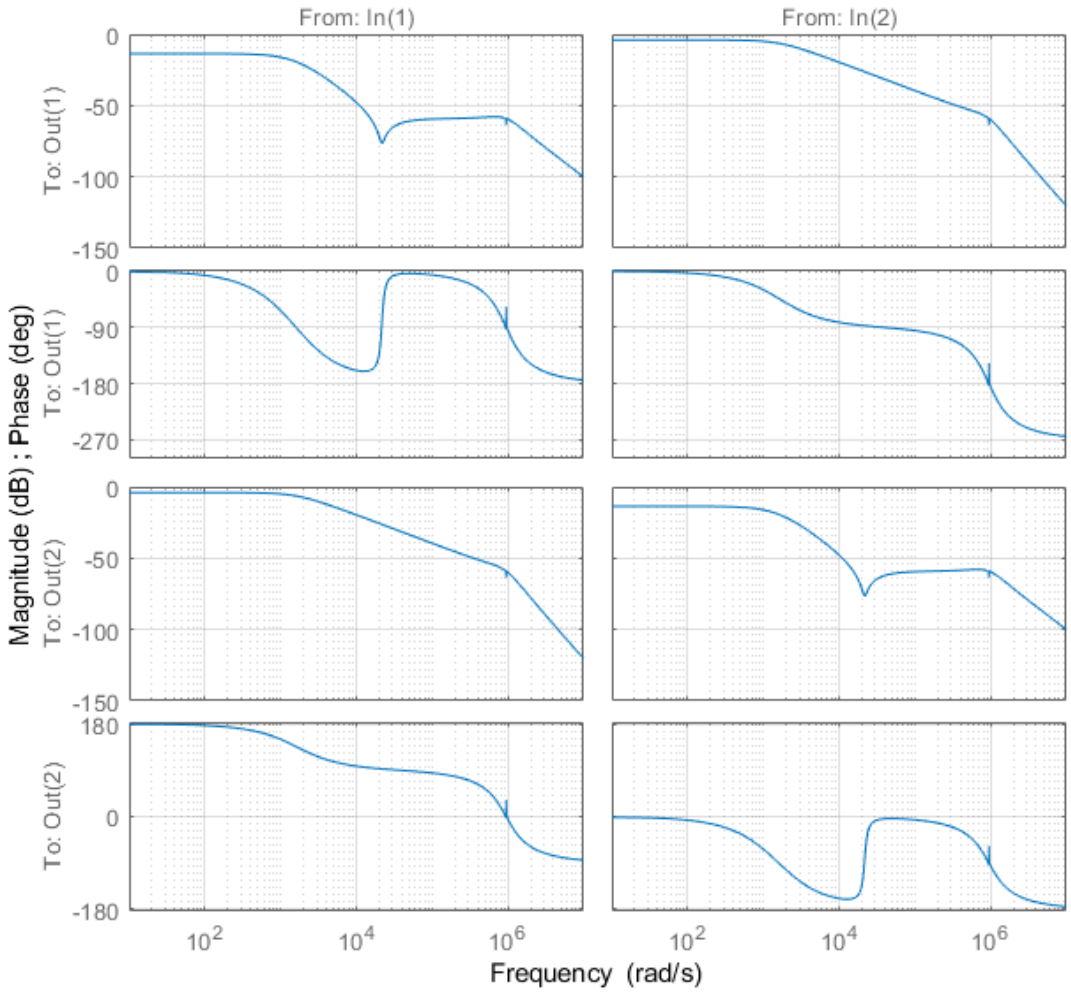

Figure 3.12: Bode plot of the filtered system. The peak is flattened by the notch filter H

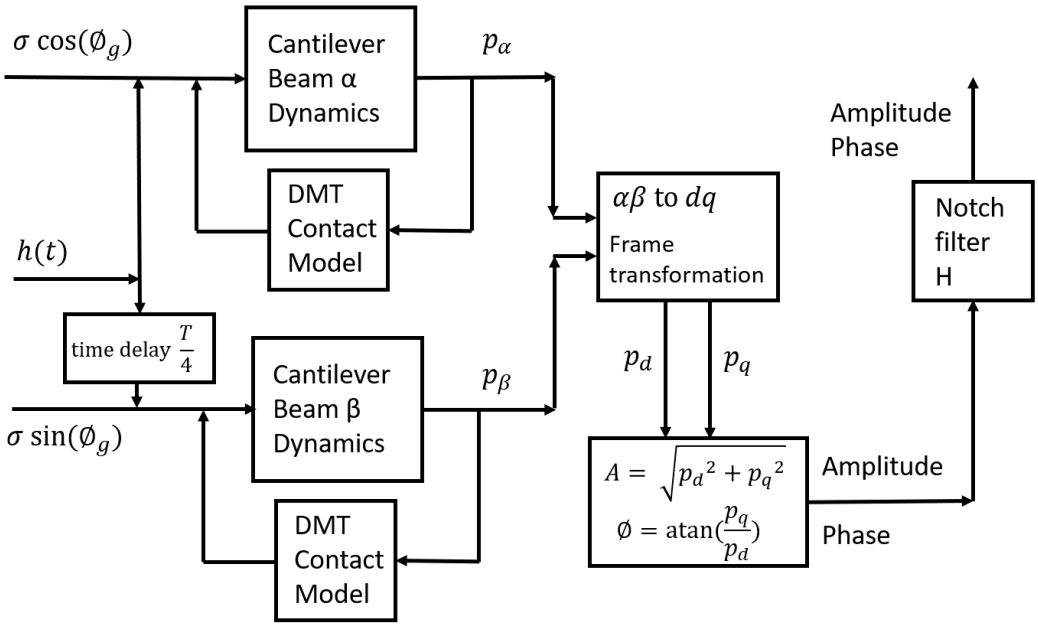

Figure 3.13: Block diagram of the Simulink simulation setup with the notch filter connected at the output

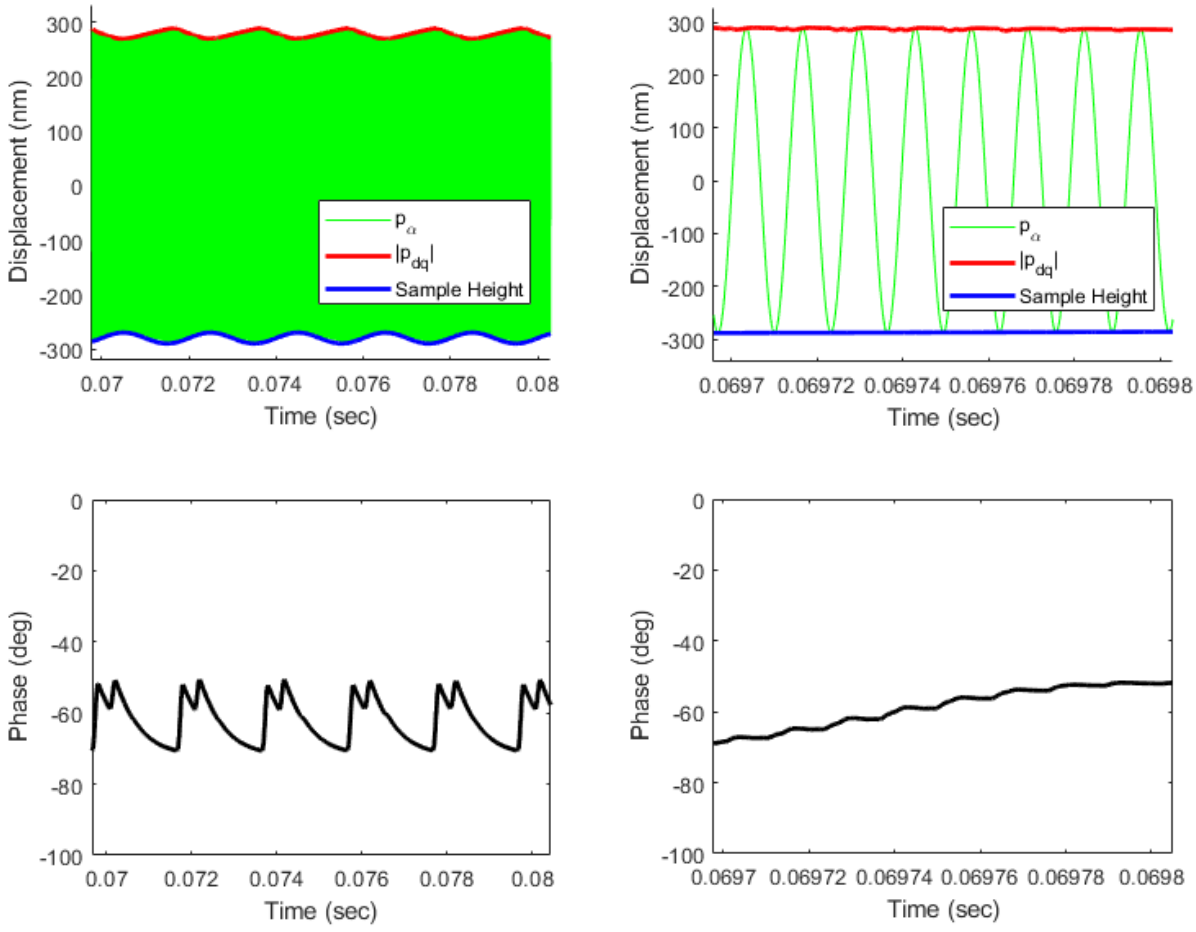

(a) general view

(b) zoomed-in view

Figure 3.14: Filtered simulation results with heights oscillating between 10 nm and 30 nm at 1000 Hz

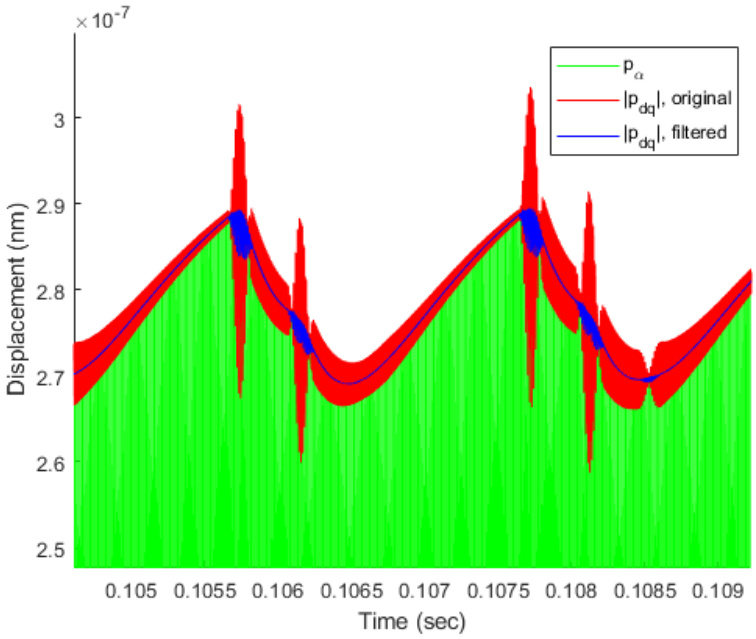

Figure 3.15: A close in comparison of filtered model and unfiltered model with heights oscillating between 10 nm and 30 nm at 1000 Hz

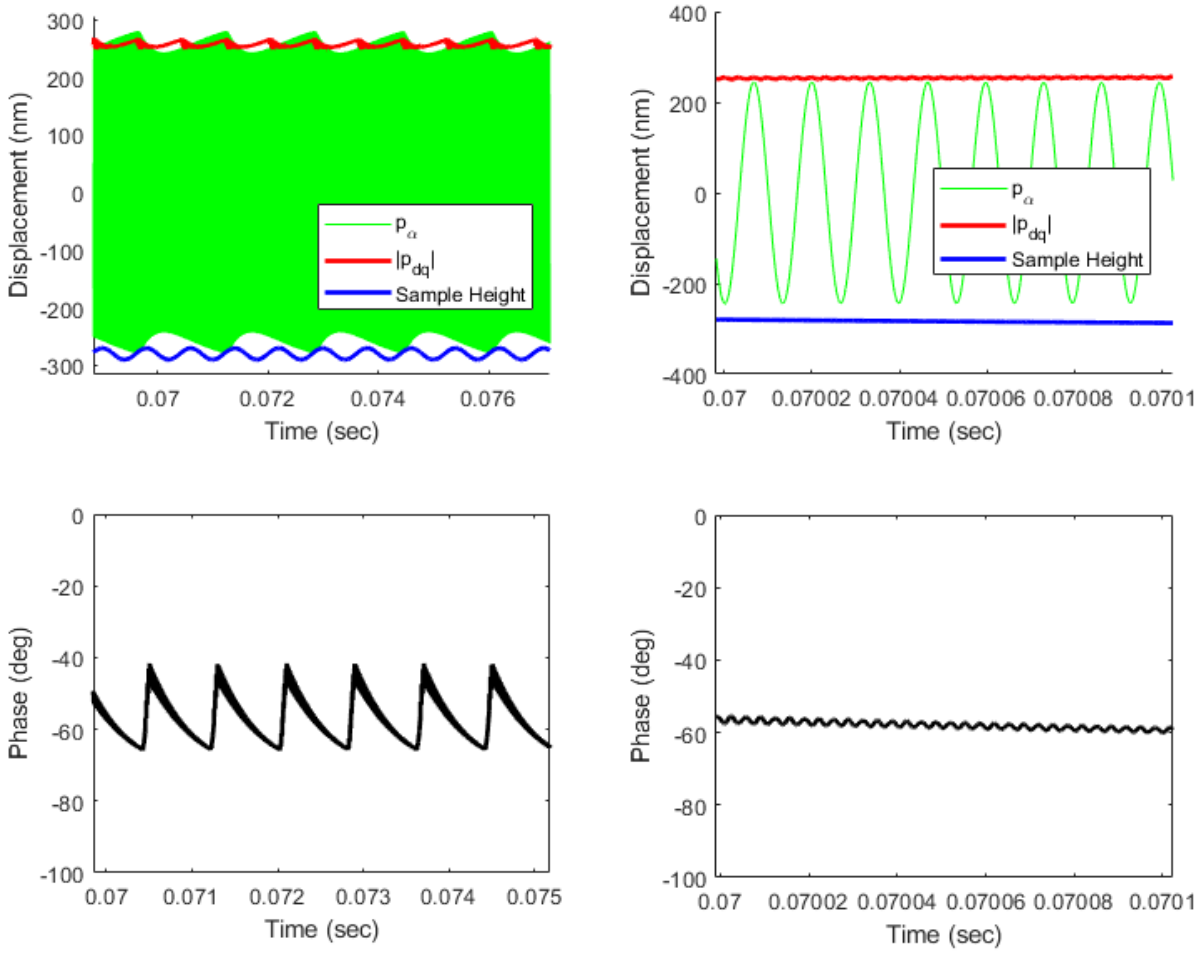

(a) general view

(b) zoomed-in view

Figure 3.16: Filtered simulation results with heights oscillating between 10 nm and 30 nm at 2500 Hz

CHAPTER 4

CONCLUSION AND FUTURE DIRECTIONS

This thesis discusses an alternative method to model the cantilever amplitude and phase dynamics in atomic force microscopy (AFM). Traditional models that relate amplitude and phase dynamics to sample motions and sample features are either too complex or inaccurate to be feasible for control design. Accordingly the regulation of tip-sample interaction force in amplitude-modulation atomic force microscopy (AM-AFM) is achieved using model-free control designs, such as proportional-integral-derivative (PID) designs. These designs, being model-free require sufficient tuning, and are limited in terms of guaranteeing stability and bandwidth. In our work, we propose modeling the cantilever dynamics of AM-AFM, which is extended with the dynamics of a fictitious cantilever, in a rotating (direct-quadrature (dq)) frame. The main feature of this approach is that the cantilever amplitude-phase dynamics can be derived from a model with a simple structure - a linear system with a non-linear tip-sample interaction term. In fact the cantilever displacement dynamics in the fixed frame has this structure and our approach preserves this structure. Accordingly amplitude and phase can be determined relatively easily using this structure. This simplicity is achieved at the price of extending the state-space with a mirror (fictitious) cantilever system, where the additional states represent another cantilever with the same properties albeit is forced with a dither forcing that has phase lag of $\pi/2$ radians compared to the real one. We show that the amplitude A and phase ϕ of the oscillating cantilever are closely related to the states p_d and p_q that describe cantilever motion in the rotating (dq) frame. In fact for a cantilever with pure sinusoidal forcing, we show that $p_d = A\cos\phi$ and $p_q = A\sin\phi$. This relations approximately even in the case when tip-sample interactions act as a forcing term on the cantilever.

We have demonstrated the efficacy of our model through detailed simulations, where we have shown that our estimate of amplitude dynamics closely follows the real amplitude for sample features varying up to bandwidth 2 kHz = 2.5% of cantilever resonance frequency. A noise frequency $> 2\omega$, where ω is the input dither frequency is observed to corrupt our estimate. We have proposed a filtered version of our original estimate signal to get alleviate this drawback. We designed a notch filter is also shown to reduce the extra high frequency signals

come from dq-frame transformation. The given filter can reduce the unwanted high frequency signals to less than 16% of the original amount and making the amplitude estimation more accurate.

The proposed approach is that the term that represents sample motion appears inside the unknown nonlinear term that represents the tip-sample interaction. Accordingly linearizing the system about a reference trajectory can be considered as an approach for control design. Such a design will result in linear control systems with matched uncertainties and unknown parameters - reflective of the unknown tip-sample interaction. Adaptive control designs, such as model-reference adaptive control and L1-adaptive control design [15] can be applied.

Another advantage with this model is on the sample physical property estimation side. Some effort was done to measure more material properties of the sample than only the topography of the sample using AM-AFM, such as [6][7][8]. Most of them relying on acquiring more information besides the amplitude and phase from the first harmonics of cantilever oscillation, and most methods are limited to materials that can create enough deformation during the measuring process, like very soft polymers or biological tissues. With the model in Equation 3.11, all terms are explicit terms, and tip-sample interaction forces can be retrieved from other signals. Sample physical properties can be estimated under more different situations, and the estimation process can be easily done in parallel with the control systems running. [13] shows an example with estimating material properties in parallel with control systems using one estimation block under the situation of model based control of AFM.

REFERENCES

[1] Srinivasa M. Salapaka, Murti V. Salapaka, *Scanning Probe Microscopy*. IEEE Control Systems Magazine, Volume 28, No. 2, Pages 65-83, April 2008.

[2] Ricardo García, Alvaro San Paulo, *Attractive and repulsive tip-sample interaction regimes in tapping-mode atomic force microscopy*. Physical Review B, Volume 60, Issues 7, Pages 4961-4967, August 1999

[3] S. I. Lee, S. W. Howell, A. Raman, R. Reifenberger, *Nonlinear dynamics of microcantilevers in tapping mode atomic force microscopy: A comparison between theory and experiment*. Physical Review B, Volume 66, Issues 11, Pages 115409, September 2002

[4] Chi Bum Lee, *Control-systems based analysis and design methods for scanning probe microscopy*. University of Illinois at Urbana-Champaign, Ph.D. Dissertation, 2010

[5] Tomás R. Rodríguez and Ricardo García *Tip motion in amplitude modulation (tapping-mode) atomic-force microscopy: Comparison between continuous and point-mass models*. Applied Physics Letters, Volume 80, No. 9, Pages 1646-1648, 2002

[6] Shuiqing Hu, Arvind Raman, *Inverting amplitude and phase to reconstruct tipsample interaction forces in tapping mode atomic force microscopy*. Nanotechnology, Volume 19, Number 37, August 2008

[7] A. Raman, S. Trigueros, A. Cartagena, A. P. Z. Stevenson, M. Susilo, E. Nauman, S. Antoranz Contera, *Mapping nanomechanical properties of live cells using multi-harmonic atomic force microscopy*. Nature Nanotechnology Volume 6, Pages 809814, November 2011

[8] Alexander X. Cartagena-Rivera, Wen-Horng Wang, Robert L. Geahlen, Arvind Raman, *Fast, multi-frequency and quantitative nanomechanical mapping of live cells using the atomic force microscope*. Scientific Reports, Volume 5, Article number: 11692, June 2015

[9] Amirnaser Yazdani, Reza Iravani, *Voltage-Sourced Converters in Power Systems: Modeling, Control and Applications*. John Wiley & Sons, Inc., 2010

[10] Gayathri Mohan, Chibum Lee, Srinivasa M. Salapaka, *Control techniques for high-speed dynamic mode imaging in atomic force microscopes*. 2011 50th IEEE Conference on Decision and Control and European Control Conference, Pages 651-656, Orlando, FL, 2011

[11] Srinivasa M. Salapaka, *Toward a new high-speed dynamic mode imaging in atomic force microscopy*. Workshop on Dynamics and Control of Micro and Nanoscale Systems, The University of Newcastle, NSW, Australia, February 2012, Powerpoint Presentation

[12] Alireza Askarian, Mayank Baranwa, Srinivasa M. Salapaka, *Droopless active and reactive power sharing in parallel operated inverters in islanded microgrids*. IEEE Conference on Decision and Control (CDC), Pages 3427-3432, Miami Beach, FL, 2018

[13] Gayathri Mohan, Chibum Lee, Srinivasa M. Salapaka, *High-bandwidth scanning of sample properties in atomic force microscopy*. 50th IEEE Conference on Decision and Control and European Control Conference, Pages 651-656, Orlando, FL, 2011

[14] Amir Moshar, *Force Measurements in AFM*. Asylum Research Atomic Force Microscopy (AFM) Workshop, Purdue University, West Lafayette, IN, Feb 2011, https://nanohub.org/resources/11018

[15] Naira Hovakimyan, Chengyu Cao, *L1 Adaptive Control Theory: Guaranteed Robustness with Fast Adaptation*. Society for Industrial and Applied Mathematics, USA. 2010